aerospace

MDPI

Article

Nonlinear Dynamics of a Space Tensioned Membrane Antenna during Orbital Maneuvering

Yifan Lu [1,2], Qi Shao [2,*], Liangliang Lv [1], Guangqiang Fang [1] and Honghao Yue [2,*]

1 Space Structure and Mechanism Technology Laboratory, China Aerospace Science and Technology Group Co., Ltd., Shanghai 201108, China
2 State Key Laboratory of Robotics and System, Harbin Institute of Technology, Harbin 150001, China
* Correspondence: sharonqs@stu.hit.edu.cn (Q.S.); block@hit.edu.cn (H.Y.)

Abstract: Due to the super flexibility and strong nonlinearity of space membrane antennas, the dynamic response of a space membrane antenna will be affected by the rigid–flexible coupling effect in the process of orbital maneuvering. In this case, the dynamic model of a tensioned membrane antenna is significantly different from that under the general condition (fixed boundary). In this study, a nonlinear dynamic model of a tensioned space membrane antenna experiencing maneuvering is established, and the influence of the rigid–flexible coupling effect on structural stiffness and damping characteristics is described. Through a numerical solution, the effects of rigid body motion and structural natural frequency on the rigid–flexible coupling effect are discussed. The results show that the vibration frequency and amplitude of the antenna are positively correlated with the acceleration and initial velocity of rigid body motion. With the increase of the natural frequency of the antenna, the vibration frequency increases but the amplitude decreases. The rigid–flexible coupling nonlinear dynamic model proposed in this work is more applicable in intelligent vibration control compared to finite element software.

Keywords: tensioned membrane antenna; nonlinearity; rigid–flexible coupling; orbital maneuvering

check for updates

Citation: Lu, Y.; Shao, Q.; Lv, L.; Fang, G.; Yue, H. Nonlinear Dynamics of a Space Tensioned Membrane Antenna during Orbital Maneuvering. *Aerospace* **2022**, *9*, 794. https://doi.org/10.3390/aerospace9120794

Academic Editor: Hekmat Alighanbari

Received: 24 October 2022
Accepted: 4 December 2022
Published: 4 December 2022

1. Introduction

Due to its low cost, lightweight, and high deployment ratio properties, the space membrane antenna can realize high-resolution observation of the earth with an extremely light load, which has become a promising antenna structure in radar remote sensing. However, the space membrane antenna also shows strong nonlinearity and flexibility, which makes its dynamic characteristics complex and vulnerable to external interference. The adjustment of its attitude and observation angle to the earth is one of the main factors causing the disturbance of its surface shape. Under the rigid–flexible coupling effect, the rigid body motion of the whole structure will have a great influence on the working performance of the space membrane antenna.

The nonlinear dynamics and response of membrane structures have been systematically studied in recent years. Zheng et al. [1–3] investigated the free and forced nonlinear vibration responses of membranes under large displacement based on power series method, multiple scale perturbation method and Lindstedt Poincaré perturbation method. The results were compared with those under small displacement. Liu et al. [4,5] established the nonlinear dynamic models of large amplitude vibration of membranes by Krylov–Bogolubov–Mitropolsky (KBM) perturbation method and homology perturbation method (HPM), and proved the high efficiency of HPM by solving the model. Sunny et al. [6] developed the dynamic equation of tensioned membranes under lateral dynamic load by using Adomian decomposition method. Fang et al. [7] established a two-variable-parameter membrane model and solved the natural frequencies and mode shapes of the membrane antenna by distributed transfer function method (DTFM). Liu et al. [8–10] conducted a series of studies on clamped membranes and tensioned space membrane antennas based on the modal assumption method and nonlinear finite element method. However, in the majority of the current researches, the membrane structures are assumed to have fixed boundaries, or the frames of the membrane antennas are fixed. In addition, the exciting forces on the membranes are always assumed to be local harmonic excitations or pulse excitations on the membrane surfaces. However, when the satellite/antenna adjusts attitude, the rigid motion of the satellite may cause the vibration of the membrane antenna because of its strong flexibility. Few studies have been done on these issues. Therefore, it is of great value to study the rigid–flexible coupling nonlinear dynamic characteristics of space membrane antennas under attitude adjustment disturbance.

At present, there are few researches on the rigid–flexible coupling dynamic characteristics of space membrane structures. In most studies, the space flexible accessories are simplified to flexible rod, beam and thin plate structures. Zhang and Deng et al. [11,12] established the rigid–flexible coupling finite element model of a spatial curved beam, taking into account the interaction between 'rigid' and 'flexible'. Yoo et al. [13] studied the influence of the motion-induced stiffness variation on the dynamic response of the plate, which is neglected in the conventional linear modeling method. Based on continuum mechanics, Fan et al. [14] deduced the dynamic equations of a rotating flexible rectangular plate by using the Lagrange equation of the second type, and compared the first-order model with the zero-order model. Yuan et al. [15] analyzed the coupling effect of translation and rotation of solar panels. Based on Hamilton's principle, Liu et al. [16] regarded solar panels as thin plates, established a discrete dynamic model through the global coordinate method, and compared it with the simulation results. Some other studies focus on the impact of the dynamic response of space membrane structures on satellites or other satellite accessories. Li et al. [17] established the rigid–flexible coupling dynamic model of a solar sail. The dynamic responses of the hub tips under different maneuvering processes and different light pressures are calculated. Zhang et al. [18] analyzed the influence of solar sail vibration on satellite orbit, attitude and its control torque through a rigid–flexible coupling model. Considering the Von-Karman nonlinear strain–displacement relationship of the solar sail, Liu et al. [19] studied the influence of its rigid–flexible coupling effects on the pitching motion of the satellite.

There are also researches which put emphasis on model identification and the nonlinear behavior of nonlinear vibrations. Song et al. [20] realized the model updating based on nonlinear normal modes extracted from vibration data via Bayesian interference. Luis et al. [21] took an algebraic approach to identify the parameters of a class of nonlinear vibration, with Hilbert transformation criterion and calculus of Mikusinski applied. Habib et al. [22] explored the relationships between nonlinear damping and isolated resonance curves. This work, by contrast, focuses on dynamic modelling of objects with a high degree of freedom, such as membrane antenna and investigates the rigid–flexible coupling effect during maneuvering of space appendages. The results can facilitate the intelligent control of large and complicated structures.

In this study, the rigid–flexible coupling nonlinear dynamic model of the space membrane antenna is established first using the finite element method. Then, based on the established model, the influences of rigid body motion and structural fundamental frequency on the dynamic response of the membrane antenna under a large range of rigid body motion are analyzed through several numerical examples. The results of this work lay a theoretical foundation for the in-orbit vibration suppression of membrane structures. Additionally, in contrast to the black-box-like operation of commercial finite element software, the proposed model can guide intelligent vibration control agent training, helping the finite element method play a role in the control of large and complex structures such as membrane antennas.

2. Nonlinear Dynamic Modeling of a Tensioned Membrane Antenna

Figure 1 shows the schematic diagram of an in-orbit satellite with a deployable membrane antenna. Usually, the cutting lace of the membrane (see Figure 1a) is to avoid wrinkles at the edge of the membrane, but this will introduce complex boundary conditions of the membrane. When the stress distribution on the membrane is relatively uniform, the lace will have little influence on the mode shape and frequency of the membrane structure [23]. Therefore, in the modeling process, the lace-free tensioned membrane antenna, as shown in Figure 1b, is adopted, which can simplify the boundary conditions. The membrane antenna consists of the thin-walled frame, the cables and the membrane. The whole structure is placed in the Cartesian coordinate system and the geometric parameters of each part are shown in Figure 1b. In this section, the geometric nonlinearity and the rigid–flexible coupling effect of the space membrane antenna will be described, respectively.

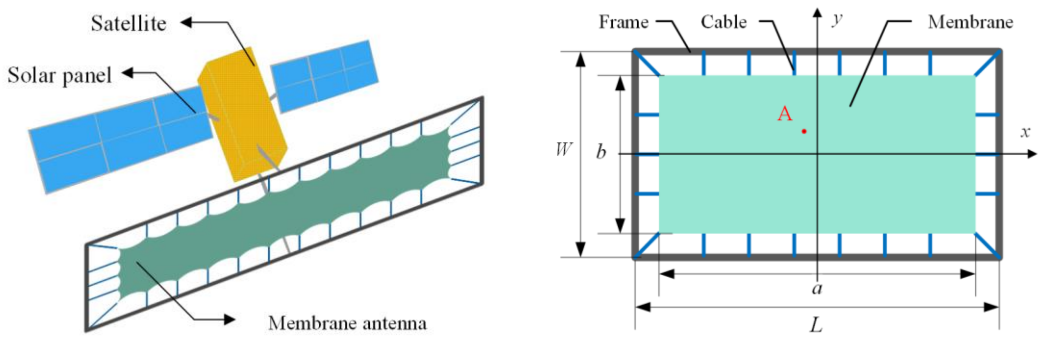

(**a**) (**b**)

Figure 1. Schematic diagram of the in-orbit satellite with a membrane antenna. (**a**) The satellite and its membrane antenna (**b**) Schematic diagram of the membrane antenna.

2.1. Finite Element Model of the Membrane Antenna

In this paper, the finite element method is used to establish the dynamic model of the membrane antenna. The thin-walled frame, cable, and membrane are, respectively, equivalent to the Euler–Bernoulli beam element, pre-tensioned rod element and triangular membrane element. In this section, the displacement field of each element is shown in details.

For the thin-walled Euler–Bernoulli beam element, it is assumed that each node of the frame has six spatial degrees of freedom: a three-axis displacement u_b, v_b, w_b and a three-axis rotation θ_{bx}, θ_{by}, θ_{bz}. Its displacement field δ_b can be expressed by element shape function $\boldsymbol{N}_b$ and element node displacement $\boldsymbol{q}_b$ as follows:

$$\delta_b = \begin{bmatrix} u_b \\ v_b \\ w_b \\ \theta_{bx} \end{bmatrix} = \begin{bmatrix} \boldsymbol{N}_{b1} \\ \boldsymbol{N}_{b2} \\ \boldsymbol{N}_{b3} \\ \boldsymbol{N}_{b4} \end{bmatrix} \cdot \boldsymbol{q}_b = \boldsymbol{N}_b \cdot \boldsymbol{q}_b \tag{1}$$

$$\boldsymbol{N}_b = \begin{bmatrix} \phi_1(e) & & & & & & \phi_2(e) & & & & & \\ & \phi_3(e) & & & & \phi_4(e) & & \phi_5(e) & & & & \phi_6(e) \\ & & \phi_3(e) & & -\phi_4(e) & & & & \phi_5(e) & & -\phi_6(e) & \\ & & & \phi_1(e) & & & & & & \phi_2(e) & & \end{bmatrix} \tag{2}$$

$$\begin{cases} \phi_1(e) = 1 - e & \phi_3(e) = 1 - 3e^2 + 2e^3 & \phi_5(e) = 3e^2 - 2e^3 \\ \phi_2(e) = e & \phi_4(e) = l\left(e - 2e^2 + e^3\right) & \phi_6(e) = l\left(e^3 - e^2\right) \end{cases} \tag{3}$$

where l is the axial length of frame element, and e is the ratio of x to l.

For the pretensioned cable element, it is assumed that each node of the cable has three spatial degrees of freedom: three-axis displacement u_c, v_c, w_c. Its displacement field $\boldsymbol{\delta}_c$ can be expressed by element shape function $\boldsymbol{N}_c$ and element node displacement $\boldsymbol{q}_c$ as follows:

$$\boldsymbol{\delta}_c = \begin{bmatrix} u_c \\ v_c \\ w_c \end{bmatrix} = \begin{bmatrix} \boldsymbol{N}_{c1} \\ \boldsymbol{N}_{c2} \\ \boldsymbol{N}_{c3} \end{bmatrix} \cdot \boldsymbol{q}_c = \boldsymbol{N}_c \cdot \boldsymbol{q}_c \tag{4}$$

$$\boldsymbol{N}_c = \begin{bmatrix} 1-e & & & e & & \\ & 1-e & & & e & \\ & & 1-e & & & e \end{bmatrix} \tag{5}$$

where e is the ratio of x to the axial length of cable element.

For the triangle membrane element, it is assumed that each node of the frame has three spatial degrees of freedom u_m, v_m, w_m. Its displacement field $\boldsymbol{\delta}_m$ can be expressed by element shape function $\boldsymbol{N}_m$ and element node displacement $\boldsymbol{q}_m$ as follows:

$$\boldsymbol{\delta}_m = \begin{bmatrix} u_m \\ v_m \\ w_m \end{bmatrix} = \begin{bmatrix} \boldsymbol{N}_{m1} \\ \boldsymbol{N}_{m2} \\ \boldsymbol{N}_{m3} \end{bmatrix} \cdot \boldsymbol{q}_m = \boldsymbol{N}_m \cdot \boldsymbol{q}_m \tag{6}$$

$$\boldsymbol{N}_m = \begin{bmatrix} \boldsymbol{N}_{m1} \\ \boldsymbol{N}_{m2} \\ \boldsymbol{N}_{m3} \end{bmatrix} = \begin{bmatrix} L_i & & & L_j & & & L_m & & \\ & L_i & & & L_j & & & L_m & \\ & & L_i & & & L_j & & & L_m \end{bmatrix} \tag{7}$$

where L_i, L_j, L_m are the area coordinates of a point in membrane element.

The following derivation and modelling are based on the finite element method, using the stated displacement fields.

2.2. Geometric Nonlinearity of the Membrane Antenna

In this paper, it is considered that flexible and thin-walled structures experience large displacement, but the relative deformation inside the element is still limited to small deformation, that is, the large displacement and small deformation problem. Taking second-order effect into consideration, geometric nonlinearity of the antenna will be described by geometric equations, physical equations and element potential energy. It has to be noted that gravitational potential energy is not included, as the membrane antenna is mostly applied in space.

2.2.1. Nonlinear Description of the Frame Element

Regarding the deformation of the frame element as a large displacement but finite rotation, the strain field of the frame beam element can be written as

$$\boldsymbol{\varepsilon}_b = \begin{bmatrix} \varepsilon_{bx} \\ \varepsilon_{by} \\ \varepsilon_{bz} \\ \varphi_{bx} \end{bmatrix} = \begin{bmatrix} \frac{\partial u_b}{\partial x} + \frac{1}{2}\left(\frac{\partial v_b}{\partial x}\right)^2 + \frac{1}{2}\left(\frac{\partial w_b}{\partial x}\right)^2 \\ y\frac{\partial^2 v_b}{\partial x^2} \\ z\frac{\partial^2 w_b}{\partial x^2} \\ \frac{\partial \theta_{bx}}{\partial x} \end{bmatrix} = \left(\boldsymbol{B}_{bl} + \frac{1}{2}\boldsymbol{I}_4^T \boldsymbol{q}_b^T \boldsymbol{B}_{bn}^T \boldsymbol{B}_{bn}\right)\boldsymbol{q}_b \tag{8}$$

where

$$\boldsymbol{B}_{bl} = \begin{bmatrix} \boldsymbol{N}'^T_{b1} & y\,\boldsymbol{N}''^T_{b2} & z\,\boldsymbol{N}''^T_{b3} & \boldsymbol{N}'^T_{b4} \end{bmatrix}^T \tag{9}$$

$$\boldsymbol{B}_{bn} = \begin{bmatrix} \boldsymbol{N}'^T_{b2} & \boldsymbol{N}'^T_{b3} \end{bmatrix}^T \tag{10}$$

$$\boldsymbol{I}_4 = \begin{bmatrix} 1 & 0 & 0 & 0 \end{bmatrix} \tag{11}$$

where $\boldsymbol{B}_{bl}$ and $\frac{1}{2}\boldsymbol{I}_4^T\boldsymbol{q}_b^T\boldsymbol{B}_{bn}^T\boldsymbol{B}_{bn}$ are linear and nonlinear geometric matrixes of the frame beam element, respectively. It is considered that the material of the structure is linear elastic and isotropic. According to generalized Hooke's law, the constitutive relation of the beam element is

$$\boldsymbol{\sigma}_b = \boldsymbol{D}_b\boldsymbol{\varepsilon}_b = \begin{bmatrix} E_b & & & \\ & E_b & & \\ & & E_b & \\ & & & G_b \end{bmatrix}\left(\boldsymbol{B}_{bl} + \frac{1}{2}\boldsymbol{I}_4^T\boldsymbol{q}_b^T\boldsymbol{B}_{bn}^T\boldsymbol{B}_{bn}\right)\boldsymbol{q}_b \tag{12}$$

where $\boldsymbol{\sigma}_b$ is the element stress field, $\boldsymbol{D}_b$ is the elastic matrix of frame element, E_b is the Young's modulus of the material, and G_b is the shear modulus of the material. Taking the variation of the element potential energy and then integrating it over time gives

$$\int_{t_1}^{t_2} \delta\Pi_b^e \mathrm{d}t = \int_{t_1}^{t_2} \frac{1}{2}\int_\Omega \boldsymbol{\sigma}_b^T\boldsymbol{\varepsilon}_b \mathrm{d}\Omega\mathrm{d}t = \int_{t_1}^{t_2} \delta\boldsymbol{q}_b^T(\boldsymbol{K}_{bl} + \boldsymbol{K}_{bn})\boldsymbol{q}_b\mathrm{d}t \tag{13}$$

where $\boldsymbol{K}_{bl}$ and $\boldsymbol{K}_{bn}$ are linear and nonlinear part of the stiffness matrix of the beam element, respectively, which can be expressed as

$$\boldsymbol{K}_{bl} = \int_\Omega \boldsymbol{B}_{bl}^T\boldsymbol{D}_b\boldsymbol{B}_{bl}\mathrm{d}\Omega \tag{14}$$

$$\begin{aligned} \boldsymbol{K}_{bn} = \; & \int_\Omega \boldsymbol{B}_{bn}^T\boldsymbol{B}_{bn}\boldsymbol{q}_b\boldsymbol{I}_4\boldsymbol{D}_b\boldsymbol{B}_{bl}\mathrm{d}\Omega + \tfrac{1}{2}\int_\Omega \boldsymbol{B}_{bl}^T\boldsymbol{D}_b\boldsymbol{I}_4^T\boldsymbol{q}_b^T\boldsymbol{B}_{bn}^T\boldsymbol{B}_{bn}\mathrm{d}\Omega \\ & + \tfrac{1}{2}\int_\Omega \boldsymbol{B}_{bn}^T\boldsymbol{B}_{bn}\boldsymbol{q}_b\boldsymbol{I}_4\boldsymbol{D}_b\boldsymbol{I}_4^T\boldsymbol{q}_b^T\boldsymbol{B}_{bn}^T\boldsymbol{B}_{bn}\mathrm{d}\Omega \end{aligned} \tag{15}$$

2.2.2. Nonlinear Description of the Cable Element

Since the cable extends only in the axial direction, only axial strain is considered in its strain field. In case of large displacement nonlinearity, the relationship between strain and displacement of cable element is similar to that of the frame beam element, which can be written as

$$\varepsilon_{cs} = \frac{\partial s_c}{\partial x} = \frac{\partial u_c}{\partial x} + \frac{1}{2}\left(\frac{\partial v_c}{\partial x}\right)^2 + \frac{1}{2}\left(\frac{\partial w_c}{\partial x}\right)^2 \tag{16}$$

where s_c denotes the nodal axial displacement, $\partial u_c/\partial x$ is the strain of the element in x direction, ε_{cs} is the axial strain, including the geometric nonlinearity caused by the lateral displacement. Then the axial strain of the cable element can be written as

$$\boldsymbol{\varepsilon}_{cs} = \left(\boldsymbol{B}_{cl} + \frac{1}{2}\boldsymbol{q}_c^T\boldsymbol{B}_{cn}^T\boldsymbol{B}_{cn}\right)\boldsymbol{q}_c \tag{17}$$

where

$$\boldsymbol{B}_{cl} = \boldsymbol{N'}_{c1} \tag{18}$$

$$\boldsymbol{B}_{cn} = \begin{bmatrix} \boldsymbol{N'}_{c2}^T & \boldsymbol{N'}_{c2}^T \end{bmatrix}^T \tag{19}$$

where $\boldsymbol{B}_{cl}$ and $\boldsymbol{B}_{cn}$ are the linear geometric matrix of the cable element and the nonlinear geometric matrix caused by the second-order effect. Considering that the material of the structure is linear elastic and isotropic, according to generalized Hooke's law, the constitutive relation of the cable element is

$$\sigma_{cx} = E_c\varepsilon_{cs} \tag{20}$$

where E_c is the Young's modulus of the material. Since the cable is subject to pretension, the potential energy of the cable includes the strain energy caused by vibration and the initial elastic potential energy induced by pretension force. Taking the variation of the element potential energy and then integrating it over time gives

$$\begin{aligned}\int_{t_1}^{t_2} \delta\Pi_c^e \mathrm{d}t &= \int_{t_1}^{t_2}\left(\frac{1}{2}\int_{\Omega} \sigma_c^T \boldsymbol{\varepsilon}_c \,\mathrm{d}\Omega + \int_0^{l_c} T_{c0}\varepsilon_{cs}\mathrm{d}x\right)\mathrm{d}t \\ &= \int_{t_1}^{t_2} \delta\boldsymbol{q}_c^T(\boldsymbol{K}_{cl}+\boldsymbol{K}_{c0}+\boldsymbol{K}_{cn})\boldsymbol{q}_c\mathrm{d}t + \int_{t_1}^{t_2}\delta\boldsymbol{q}_c^T\boldsymbol{Q}_{c\Pi}\mathrm{d}t\end{aligned} \tag{21}$$

where $\boldsymbol{K}_{cl}$ and $\boldsymbol{K}_{cn}$ are linear part of the stiffness matrix of the cable element and the nonlinear part caused by the second order effect; $\boldsymbol{K}_{c0}$ denotes the equivalent stiffness matrix induced by pretension force; $\boldsymbol{Q}_{c\Pi}$ denotes the equivalent load vector induced by pretension force, which are expressed as

$$\boldsymbol{K}_{cl} = \int_{\Omega} \boldsymbol{B}_{cl}^T E_c \boldsymbol{B}_{cl}\mathrm{d}\Omega \tag{22}$$

$$\boldsymbol{K}_{cn} = \frac{1}{2}\int_{\Omega}\boldsymbol{B}_{cl}^T E_c \boldsymbol{q}_c^T \boldsymbol{B}_{cn}^T\boldsymbol{B}_{cn}\mathrm{d}\Omega + \int_{\Omega}\boldsymbol{B}_{cn}^T\boldsymbol{B}_{cn}\boldsymbol{q}_c E_c\boldsymbol{B}_{cl}\mathrm{d}\Omega + \frac{1}{2}\int_{\Omega}\boldsymbol{B}_{cn}^T\boldsymbol{B}_{cn}\boldsymbol{q}_c E_c \boldsymbol{q}_c^T\boldsymbol{B}_{cn}^T\boldsymbol{B}_{cn}\mathrm{d}\Omega \tag{23}$$

$$\boldsymbol{K}_{c0} = \int_0^{l_c}\boldsymbol{B}_{cn}^T T_{c0}\boldsymbol{B}_{cn}\mathrm{d}x \tag{24}$$

$$\boldsymbol{Q}_{c\Pi} = \int_0^{l_c} T_{c0}\boldsymbol{B}_{cl}^T\mathrm{d}x \tag{25}$$

2.2.3. Nonlinear Description of the Membrane Element

Based on Kirchhoff's thin plate hypothesis and Von Karman's nonlinear theory, the relationship between the strain and displacement field of the membrane element can be expressed as:

$$\begin{aligned}\boldsymbol{\varepsilon}_m &= \begin{bmatrix} \varepsilon_{mx} & \varepsilon_{my} & \gamma_{mxy}\end{bmatrix}^T \\ &= \begin{bmatrix} \frac{\partial u_m}{\partial x}+\frac{1}{2}\left(\frac{\partial w_m}{\partial x}\right)^2 & \frac{\partial v_m}{\partial y}+\frac{1}{2}\left(\frac{\partial w_m}{\partial y}\right)^2 & \frac{\partial u_m}{\partial y}+\frac{\partial v_m}{\partial x}+\frac{\partial w_m}{\partial x}\frac{\partial w_m}{\partial y}\end{bmatrix}^T \\ &= \left(\boldsymbol{B}_{ml}+\frac{1}{2}\boldsymbol{H}\boldsymbol{h}\right)\boldsymbol{q}_m\end{aligned} \tag{26}$$

where

$$\boldsymbol{B}_{ml} = \begin{bmatrix}\boldsymbol{N'}_{m1x}^T & \boldsymbol{N'}_{m2y}^T & \boldsymbol{N'}_{m2x}^T+\boldsymbol{N'}_{m1y}^T\end{bmatrix}^T \tag{27}$$

$$\mathrm{H} = \begin{bmatrix}\boldsymbol{N'}_{m3x}\boldsymbol{q}_m & 0 & \boldsymbol{N'}_{m3y}\boldsymbol{q}_m \\ 0 & \boldsymbol{N'}_{m3y}\boldsymbol{q}_m & \boldsymbol{N'}_{m3x}\boldsymbol{q}_m\end{bmatrix}^T \tag{28}$$

$$\mathrm{h} = \begin{bmatrix}\boldsymbol{N'}_{m3x}^T & \boldsymbol{N'}_{m3y}^T\end{bmatrix}^T \tag{29}$$

where ε_{mx}, ε_{my} and γ_{mxy} are normal stress and shear stress of the membrane element in x and y directions. $\boldsymbol{B}_{ml}$ and $\frac{1}{2}\boldsymbol{H}\boldsymbol{h}$ are the linear geometric matrix of the membrane element and the nonlinear geometric matrix generated by the interaction of in-plane and out-of-plane displacements. Since membrane structures belong to plane stress problems, the constitutive relation of the membrane element is

$$\boldsymbol{\sigma}_m = \boldsymbol{D}_m\boldsymbol{\varepsilon}_m = \frac{E_m}{1-\mu^2}\begin{bmatrix}1 & \mu & 0\\ \mu & 1 & 0\\ 0 & 0 & \frac{(1-\mu)}{2}\end{bmatrix}\boldsymbol{\varepsilon}_m \tag{30}$$

where $\boldsymbol{D}_m$ is the elastic matrix of the membrane element, E_m and μ are Young's modulus and Poisson ratio of the material, respectively. Assume that the pretension stress of the membrane element is

$$\boldsymbol{\sigma}_{m0} = \begin{bmatrix}\sigma_{mx0} & \sigma_{my0} & \tau_{mxy0}\end{bmatrix}^T \tag{31}$$

Similar to the cable element, taking the variation of the element potential energy and then integrating it over time gives

$$\begin{aligned}\int_{t_1}^{t_2} \delta\Pi_m^e \mathrm{d}t &= \int_{t_1}^{t_2} \left(\frac{1}{2}\int_\Omega \boldsymbol{\sigma}_m^T \boldsymbol{\varepsilon}_m \mathrm{d}\Omega + \int_\Omega \boldsymbol{\sigma}_{m0}^T \boldsymbol{\varepsilon}_m \mathrm{d}\Omega\right)\mathrm{d}t \\ &= \int_{t_1}^{t_2} \delta\boldsymbol{q}_m^T (\boldsymbol{K}_{ml} + \boldsymbol{K}_{m0} + \boldsymbol{K}_{mn})\boldsymbol{q}_m \mathrm{d}t + \int_{t_1}^{t_2} \delta\boldsymbol{q}_m^T \boldsymbol{Q}_{m\Pi} \mathrm{d}t\end{aligned} \tag{32}$$

where $\boldsymbol{K}_{ml}$ and $\boldsymbol{K}_{mn}$ are the linear part of the stiffness matrix of the membrane element and the nonlinear part caused by the second-order effect; $\boldsymbol{K}_{m0}$ is the equivalent stiffness matrix induced by pretension; $\boldsymbol{Q}_{m\Pi}$ is the equivalent load vector induced by pretension, which are expressed as

$$\boldsymbol{K}_{ml} = \int_\Omega \boldsymbol{B}_{ml}^T \boldsymbol{D}_m \boldsymbol{B}_{ml} \mathrm{d}\Omega \tag{33}$$

$$\boldsymbol{K}_{mn} = \frac{1}{2}\int_\Omega \boldsymbol{B}_{ml}^T \mathrm{D}_m \boldsymbol{H}\boldsymbol{h} \mathrm{d}\Omega + \int_\Omega \boldsymbol{h}^T \boldsymbol{H}^T \boldsymbol{D}_m \boldsymbol{B}_{ml} \mathrm{d}\Omega + \frac{1}{2}\int_\Omega \boldsymbol{h}^T \boldsymbol{H}^T \boldsymbol{D}_m \boldsymbol{H}\boldsymbol{h} \mathrm{d}\Omega \tag{34}$$

$$\boldsymbol{K}_{m0}\boldsymbol{q}_m = \int_\Omega \boldsymbol{h}^T \boldsymbol{H}^T \boldsymbol{\sigma}_{m0} \mathrm{d}\Omega \tag{35}$$

$$\boldsymbol{Q}_{m\Pi} = \int_\Omega \boldsymbol{B}_{ml}^T \boldsymbol{\sigma}_{m0} \mathrm{d}\Omega \tag{36}$$

2.3. Rigid–Flexible Coupling Dynamic Model of the Membrane Antenna

The dynamic model of membrane antenna will be established in terms of Hamilton's principle, which can be expressed as

$$\int_{t_1}^{t_2} (-\delta T + \delta\Pi - \delta W)\mathrm{d}t = 0 \tag{37}$$

where T is kinetic energy; Π is potential energy; and W is the work done by external force on the system. In this section, the kinematic description will be given first, and the rigid–flexible coupling dynamic model will be therefore achieved.

When the space membrane antenna works in orbit, its attitude is mainly adjusted by the angle between the reflecting surface and the ground, i.e., the rigid body motion rotating around the x axis (see Figure 1) [24]. Therefore, in this work, it is assumed that the membrane antenna rotates around the x axis at a certain initial velocity and finally stops. Kane pointed out that for the rigid–flexible coupling effect caused by large-scale rigid body motion, the coupling term introduced by the influence of rigid body motion on the dynamic characteristics of elastic motion can be captured when considering the second-order nonlinearity [25].

Based on this principle, a global coordinate system and a floating coordinate system are established on the space membrane antenna by using the mixed coordinate system method, as shown in Figure 2, where $o_g x_g y_g z_g$ is the global coordinate system, $o_{bi} x_{bi} y_{bi} z_{bi}$ is the floating coordinate system of the i-th beam on the frame, $o_{cj} x_{cj} y_{cj} z_{cj}$ is the floating coordinate system of the j-th cable, and $o_m x_m y_m z_m$ is the floating coordinate system of the membrane. The rotation angle of the membrane antenna around x axis is θ, the rotation angular velocity and angular acceleration are $\dot{\theta}$ and $\ddot{\theta}$, respectively. The position vector of the origin of the floating coordinate system in the global coordinate system is $\boldsymbol{r}_0$, and the spatial transformation matrix from floating coordinate system to global coordinate system is $\boldsymbol{A}$. Based on Hamilton's principle, the rigid–flexible coupling nonlinear dynamic model of space membrane antenna will be established in this section.

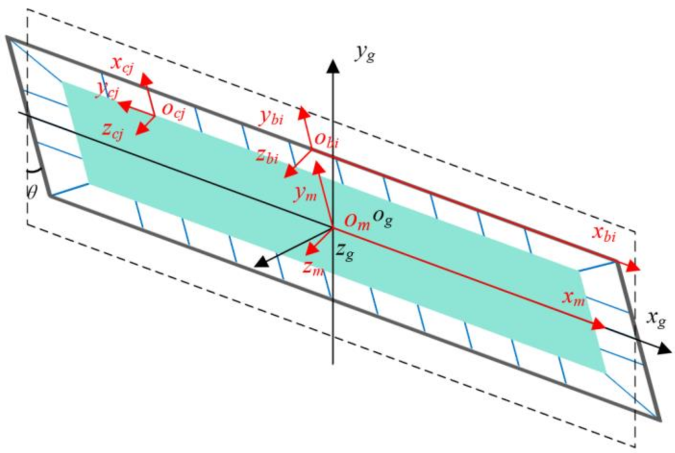

Figure 2. The coordinate systems of space membrane antenna.

The position vector $\boldsymbol{R}_p$ of an arbitrary point P on the membrane antenna in the global coordinate system can be expressed as

$$\boldsymbol{R}_p = \boldsymbol{r}_0 + \boldsymbol{A}(\boldsymbol{r}_p + \boldsymbol{N}\boldsymbol{q}) \tag{38}$$

where $\boldsymbol{r}_p$ is the position vector of point P in the floating coordinate system before elastic deformation; $\boldsymbol{N}\boldsymbol{q}$ denotes the elastic deformation of point P in the floating coordinate system. Furthermore, the velocity and acceleration vectors of point P in the global coordinate system are written as

$$\dot{\boldsymbol{R}}_p = \dot{\boldsymbol{r}}_0 + \dot{\boldsymbol{A}}(\mathrm{r}_p + \boldsymbol{N}\boldsymbol{q}) + A\boldsymbol{N}\dot{\boldsymbol{q}} \tag{39}$$

$$\ddot{\boldsymbol{R}}_p = \ddot{r}_0 + \ddot{\boldsymbol{A}}(\mathrm{r}_p + \boldsymbol{N}\boldsymbol{q}) + 2\dot{\boldsymbol{A}}\boldsymbol{N}\dot{\boldsymbol{q}} + \boldsymbol{A}\boldsymbol{N}\ddot{\boldsymbol{q}} \tag{40}$$

Taking the variation of the element kinetic energy and then integrating it over time yields

$$\begin{aligned} \int_{t_1}^{t_2} -\delta T^e \mathrm{d}t &= \int_{t_1}^{t_2} \delta\boldsymbol{q}^T \int_\Omega \rho \boldsymbol{N}^T \boldsymbol{A}^T \ddot{\boldsymbol{R}}_p \mathrm{d}\Omega \mathrm{d}t \\ &= \int_{t_1}^{t_2} \delta\boldsymbol{q}^T \left[\boldsymbol{M}\ddot{\boldsymbol{q}} + \boldsymbol{G}\dot{\boldsymbol{q}} + \boldsymbol{K}_T\boldsymbol{q} + \boldsymbol{Q}_T\right] \mathrm{d}t \end{aligned} \tag{41}$$

where $\boldsymbol{M}$ is the element mass matrix; $\boldsymbol{G}$ and $\boldsymbol{K}_T$ are the additional mass matrices caused by the rigid–flexible coupling effect, which exhibit damping and stiffness characteristics, respectively; $\boldsymbol{Q}_T$ is the external load caused by the acceleration of rigid motion. When the rigid–flexible coupling effect is not considered, $\boldsymbol{G} = \boldsymbol{K}_T = \boldsymbol{0}$, and Equation (41) degenerate to a general rigid body dynamic equation. The above matrices are specifically expressed as

$$\boldsymbol{M} = \int_\Omega \rho \boldsymbol{N}^T \boldsymbol{A}^T A\boldsymbol{N} \mathrm{d}\Omega \tag{42}$$

$$\boldsymbol{G} = 2\int_\Omega \rho \boldsymbol{N}^T \boldsymbol{A}^T \dot{\boldsymbol{A}}\boldsymbol{N} \mathrm{d}\Omega \tag{43}$$

$$\boldsymbol{K}_T = \int_\Omega \rho \boldsymbol{N}^T \boldsymbol{A}^T \ddot{\boldsymbol{A}}\boldsymbol{N} \mathrm{d}\Omega \tag{44}$$

$$\boldsymbol{Q}_T = \int_\Omega \rho \boldsymbol{N}^T \boldsymbol{A}^T \left(\ddot{\boldsymbol{r}}_0 + \ddot{\boldsymbol{A}}\boldsymbol{r}_p\right) \mathrm{d}\Omega \tag{45}$$

For fixed-axis rotation, the spatial transformation matrix $\boldsymbol{A}$ is the function of the rotation angle. Equations (43)–(45) can be turned into

$$\boldsymbol{G} = \boldsymbol{G}_p \cdot \omega(t) \tag{46}$$

$$\boldsymbol{K}_T = \boldsymbol{K}_{T1} \cdot \alpha(t) + \boldsymbol{K}_{T2} \cdot \omega^2(t) \tag{47}$$

$$\boldsymbol{q}_T = \boldsymbol{q}_{T1} \cdot \alpha(t) + \boldsymbol{q}_{T2} \cdot \omega^2(t) \tag{48}$$

where $\alpha(t)$ and $\omega(t)$ are the acceleration and velocity of rigid rotation, respectively. $\boldsymbol{G}$, $\boldsymbol{K}_{T1}$, $\boldsymbol{K}_{T2}$, $\boldsymbol{Q}_{T1}$, $\boldsymbol{Q}_{T2}$ are constant parts separated from $\boldsymbol{G}$, $\boldsymbol{K}_T$, $\boldsymbol{Q}_T$. It is clear that rigid–flexible coupling effect is relevant with acceleration and velocity, which will be discussed in details later.

In Section 2.1, the integration of potential energy of the frame, cable and membrane elements have been obtained, as shown in Equations (13), (21) and (32). The integration of kinetic energy of each element has also been obtained by using the mixed coordinate system method, as shown in Equation (40). Substituting the above equations into Equation (37), one can obtain the following rigid–flexible coupling dynamic equations of the frame beam element, the cable element, and the membrane element, respectively. By assembling the various matrices of all the elements, one can obtain the rigid–flexible coupling nonlinear dynamic equation of the space membrane antenna.

$$\boldsymbol{M}\ddot{\boldsymbol{q}} + (\boldsymbol{C} + \boldsymbol{G})\dot{\boldsymbol{q}} + (\boldsymbol{K}_0 + \boldsymbol{K}_l + \boldsymbol{K}_n + \boldsymbol{K}_T)\boldsymbol{q} + \boldsymbol{Q}_\Pi + \boldsymbol{Q}_T = \boldsymbol{F} \tag{49}$$

where the subscripts b, c and m represent the frame beam element, cable element and membrane element, respectively, and the subscripts *0*, l, n, Π and T represent the components related to pretension, linearity, nonlinearity, strain energy and rigid–flexible coupling effect, respectively. $\boldsymbol{M}$ denotes the mass matrix, $\boldsymbol{C}$ denotes the damping matrix, $\boldsymbol{F}$ denotes the external load vector, $\boldsymbol{K}$ denotes the stiffness matrix, and $\boldsymbol{Q}$ denotes the equivalent load vector.

In this section, the influence of geometric nonlinearity and rigid–flexible coupling effect on the dynamic characteristics of membrane antennas is described theoretically. Instead of a merely numerical output, the expression of the theoretical model is more helpful to understand the nonlinear and rigid–flexible coupling dynamic behavior of space membrane antenna, so as to guide the dynamic design optimization and dynamic response control of the structure.

3. Solution of Rigid–Flexible Coupling Nonlinear Dynamic Response

In this paper, the Wilson-θ method is used to solve the nonlinear dynamic equations. The model of the space membrane antenna is shown in Figure 1, and the materials and geometric parameters of the membrane antenna are shown in Table 1. Based on the obtained dynamic model, the natural frequencies of some modes of the membrane antenna, which are only related to the mass and stiffness of the antenna system, are shown in Table 2, and the shapes of the first four modes are shown in Figure 3. It should be noted that the natural frequencies are used to illustrate the basic dynamic characteristics of the membrane antenna in this section, and to make comparison with vibration frequencies to explain how the rigid–flexible coupling effect influences the response. Since the membrane antenna is a biaxially symmetrical structure, the mode shapes are symmetric or central symmetric. For the membrane antenna in this section, the first and third modes are symmetric, while the second and fourth modes are central-symmetric. Because symmetry of modes has little correlations to the research on the rigid–flexible coupling effect, emphasis will not be put on symmetry of modes in the following sections.

Assume that the antenna structure has proportional damping, $\boldsymbol{C} = \alpha\boldsymbol{M} + \beta\boldsymbol{K}$, where α and β are damping coefficients. It is considered that the membrane antenna rotates at a constant angular velocity ω_0 at first, then decelerates from a certain moment, and finally comes to a standstill after a certain period of time T. Without losing generality, an arbitrary point A with coordinates (0.7036, 0.4267) on the membrane is selected as the measuring point, as shown in Figure 1b. Firstly, we assume that the initial angular velocity $\omega_0 = \pi/5$ rad·s^{-1}, T = 1 s and $\alpha = \beta$=0.01. The membrane antenna shapes at different moments are listed in Figure 4, where the vibration displacements have been magnified 1000 times to facilitate observation. The time response of the out-of-plane displacement of point A in this process is shown in Figure 5a. It can be found that during the first second, when the membrane antenna is decelerating, because of the inertia, the vibration equilibrium point of point A is not located in the plane before the membrane is deformed. When the rigid body motion stops, the out-of-plane displacement is approximately symmetrical with respect to the original plane of the membrane. Due to the damping effect, the vibration of the structure decays rapidly after two seconds. The frequency characteristics changing with time can be obtain by 3D wavelet transformation, as seen in detail in Figure 6. The frequency reaches the peak when deceleration starts because the velocity and acceleration of rigid motion contribute to the stiffness of antenna system as Equation (49) shows. The energy rises pretty high at initial and then reduces after about one second, which corresponds with the displacement response. The frequency decreases as vibration attenuates due to the nonlinearity. The energy gradually decreases as amplitude falls off, and the stable vibration frequency fluctuates around 2 Hz, eventually.

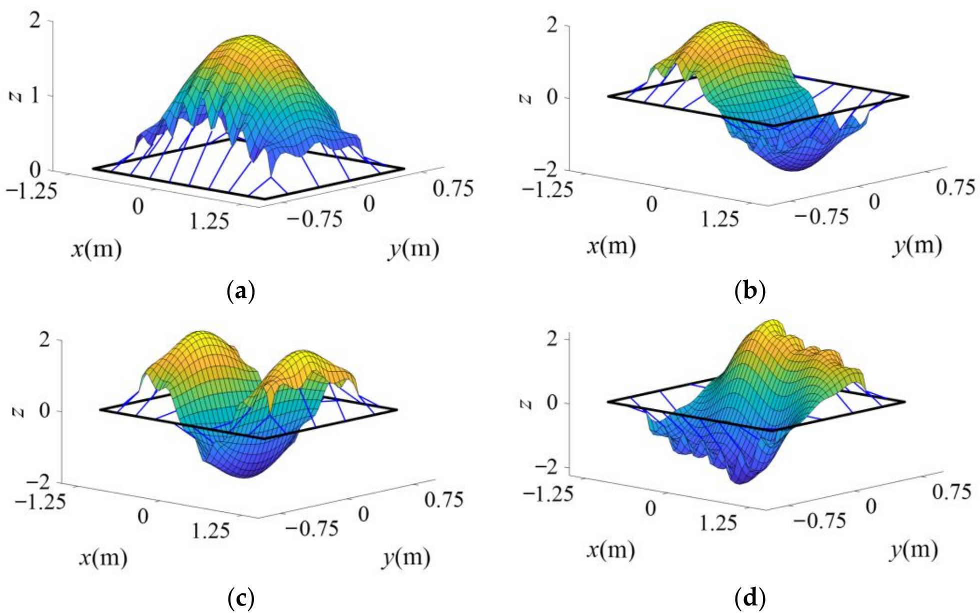

Figure 3. Mode shapes of the membrane antenna. (**a**) the 1st mode, (**b**) the 2nd mode, (**c**) the 3rd mode, (**d**) the 4th mode.

Table 1. Materials and geometric parameters of the membrane antenna.

Component	Parameter	Value
Frame	L/m	2.5
	W/m	1.5
	Young's modulus/GPa	3
	Poisson ratio	0.38
	Density/(kg·m^{-3})	1380
	Cross-sectional area/m^2	5.24×10^{-4}
	Moment of inertia on z axis/m^4	2.69×10^{-7}
	Moment of inertia on y axis/m^4	4.81×10^{-7}
Cable	Young's modulus/GPa	133
	Poisson ratio	0.36
	Density/(kg·m^{-3})	1440
	Cross-sectional area/m^2	3.14×10^{-6}
Membrane	a/m	2
	b/m	1
	Thickness/m	10^{-4}
	Young's modulus/GPa	3.5
	Poisson ratio	0.34
	Density/(kg·m^{-3})	1530

Table 2. Modal frequencies of the membrane antenna.

Mode	Frequency/Hz	Mode	Frequency/Hz
1	1.0005	6	2.1286
2	1.2498	7	2.4265
3	1.6040	8	2.4586
4	1.9923	9	2.7534
5	2.0101	10	2.9362

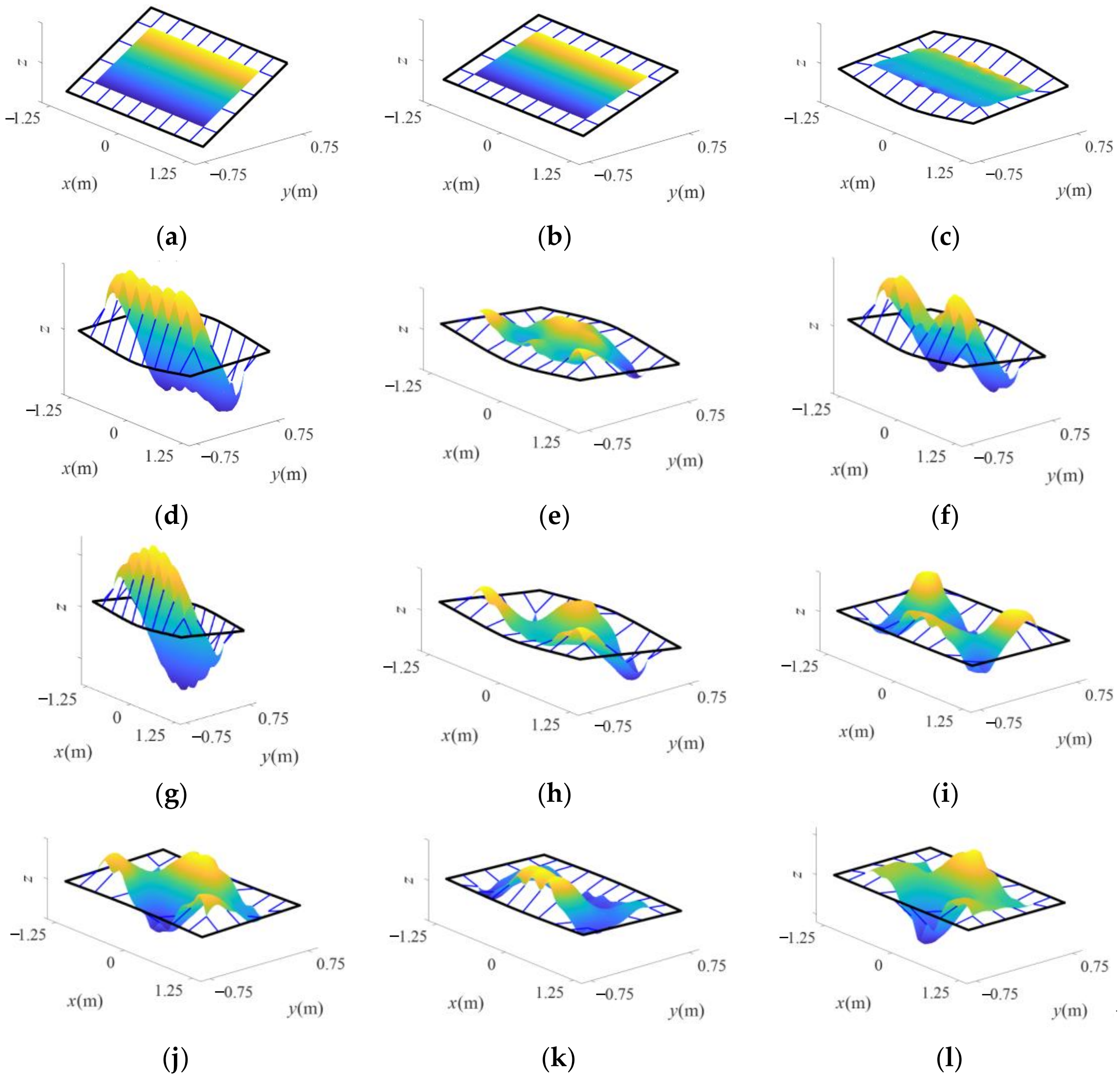

Figure 4. Shape response of the membrane antenna (ω_0 = π/5 rad/s; T = 1 s; α = β=0.01). (**a**) Uniform rotation, (**b**) start to decelerate: t = 0 s (**c**) t = 0.04 s (**d**) t = 0.15 s (**e**) t = 0.5 s (**f**) t = 0.6 s (**g**) t = 0.8 s (**h**) t = 1 s (**i**) t = 1.2 s (**j**) t = 1.4 s (**k**) t = 1.55 s (**l**) t = 1.85 s.

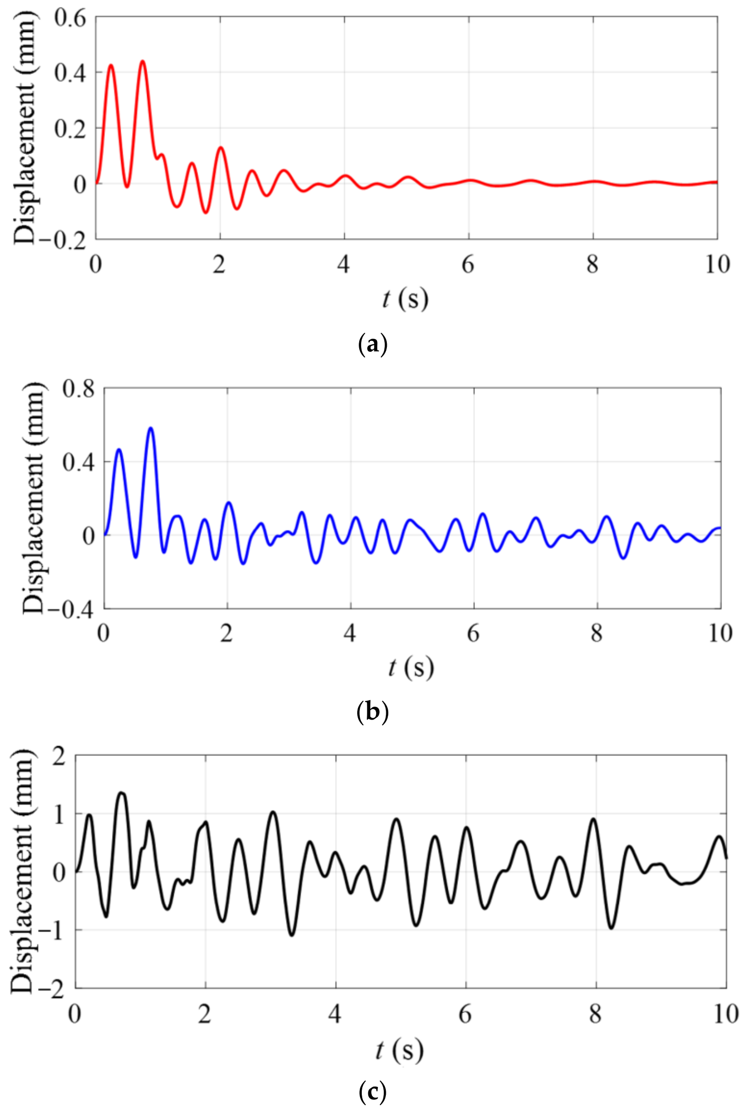

Figure 5. Time responses of the out-of-plane displacement of point A. (**a**) $\omega_0 = \pi/5$ rad/s; $T = 1$ s; $\alpha = \beta = 0.01$. (**b**) $\omega_0 = \pi/5$ rad/s; $T = 1$ s; $\alpha = \beta = 0.001$. (**c**) $\omega_0 = \pi/2$ rad/s; $T = 1$ s; $\alpha = \beta = 0.001$.

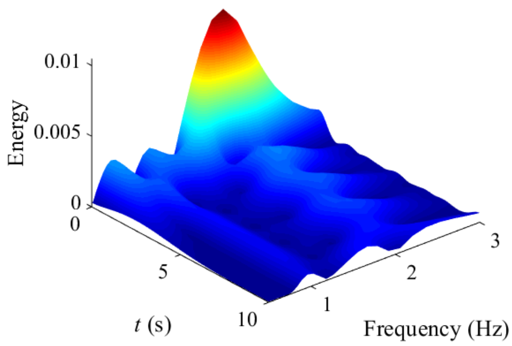

Figure 6. Time-response frequency graph ($\omega_0 = \pi/5$ rad/s; $T = 1$ s; $\alpha = \beta = 0.01$).

Then, in order to investigate the influence of the damping coefficients, set $\alpha = \beta = 0.001$. The time response of point A is shown in Figure 5b. It can be found that the attenuation of structural vibration is much slower. Then, we set $\omega_0 = \pi/2$ rad/s; the time response of point A is given in Figure 5c. It can be observed that the membrane vibration amplitude increases significantly as the initial kinetic energy increases. Moreover, the vibration of the structure has no obvious attenuation during the first ten seconds.

A series of displacement response vectors $\boldsymbol{X}_i$ can be obtained with a full-order finite element analysis employed. The proper orthogonal modes (POMs), which are the most significant contribution to the nonlinear dynamic response, are identified through proper orthogonal decomposition (POD). A set of normal modes resembling desired POMs are selected according to the modal assurance criterion. Therefore, the modal analysis of the dominant shape obtained by numerical simulation is then carried out [26].

The response vectors $\boldsymbol{X}_i$s are stored at discrete output times in the so-called snapshot matrix $\boldsymbol{X}$. A correlation matrix $\boldsymbol{R}$ could be obtained from snapshots matrix as

$$\boldsymbol{R} = \boldsymbol{X}^T\boldsymbol{X}/n \tag{50}$$

where n is the number of output time samples and N is the number of degree of freedoms. The eigen analysis is then performed on correlation matrix

$$[\boldsymbol{R} - \lambda\boldsymbol{I}]\boldsymbol{p} = 0 \tag{51}$$

where λ and p are eigenvalue and eigenvector, respectively. As in normal mode analysis, eigenvectors can illustrate the mode shape in a response, which is called a proper orthogonal mode (POM), while eigenvalues indicate the significance of their corresponding shape, which is called proper orthogonal value (POV). The larger the POV is, the more contributions the corresponding POM has made. The participation of POM can be determined by participation factor χ_i, which is

$$\chi_i = \lambda_i/\sum_{i=1}^{N}\lambda_i\,(i = 1, \cdots, N) \tag{52}$$

The sum of all participation factors should be 1. When selecting POMs with a number of M ($M < N$), the cumulative participation factors of selected POMs can be expressed as

$$\nu = \sum_{i=1}^{M}\chi_i(0 < \nu < 1) \tag{53}$$

The POMs could resemble normal modes a lot for simple structures, while they could be quite different for complex structures with high DOFs such as membrane antenna. The modal assurance criterion (MAC) is therefore applied to measure the similarity of a pair of POM and normal mode [27]. The MAC value of a pair of vectors could be written as

$$MAC(\boldsymbol{p}_k, \boldsymbol{\varphi}_l) = \frac{\left|\boldsymbol{p}_k^T\boldsymbol{\varphi}_l\right|^2}{(\boldsymbol{p}_k^T\boldsymbol{p}_k)(\boldsymbol{\varphi}_l^T\boldsymbol{\varphi}_l)}\ (k = 1, \cdots, M;\ l = 1, \cdots, N) \tag{54}$$

where $\boldsymbol{p}_k$ is one of select POMs and $\boldsymbol{\varphi}_l$ is one of normal modes. Normal modes are sorted by their MAC values, and M could be adjusted according to the cumulative participation factor.

The combined shape of POMs with a participation factor of 99% of the membrane antenna is shown in Figure 7, which is a so-called dominant shape. Table 3 offers five normal modes with the highest MAC values and their cumulative participation factor.

Table 3. The first five normal modes.

Normal Mode	4	5	23	7	51
MAC (%)	76.28	3.75	2.74	1.69	1.12
Cumulative MAC (%)			85.58		

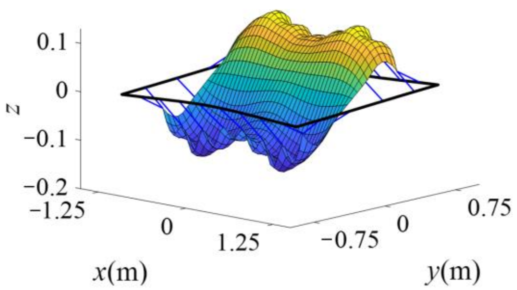

Figure 7. The dominant shape of the antenna.

It can be seen from Table 3 that the dominant mode of the membrane antenna is similar to its fourth-order mode with a similarity as high as 76.28%. Therefore, it can be considered that its mode shape is dominated by the fourth-order mode shape. However, compared with Table 2, one can find that the response frequency of the membrane antenna in Figure 5 is larger than its fourth-order frequency. This indicates that under the disturbance of rigid body motion, the dynamic response frequency of the membrane antenna is not consistent with its modal frequency of the corresponding order mode shape. The dominant mode shape is related to its rigid body motion, while its dynamic response frequency is affected by both the structure itself as well as the rigid body motion. In Section 4, we will discuss the influence of the rigid body motion on the dynamic response characteristics of the membrane antenna through multiple sets of numerical examples.

4. Discussion on Rigid–Flexible Coupling Nonlinear Dynamic Characteristics

In this section, four different case studies are carried out to analyze the dynamic response of point A in the time domain and frequency domain, and to discuss the influence of rigid body motion (acceleration, initial velocity and deceleration duration) and structural fundamental frequency on the rigid–flexible coupling dynamic response characteristics under the disturbance of antenna attitude adjustment. Three membrane antenna models of different fundamental frequencies are first obtained by adjusting the pretension forces of the cables, which are named M1, M2 and M3. The influences of the initial rotational velocity ω_0, the deceleration duration T and the corresponding acceleration on the dynamic response of three models are discussed, respectively. The frequency components of antenna vibration are extracted by FFT. Though the frequency is varying for a nonlinear vibration, the distribution of frequency components is kind of concentrated. The frequency component with highest energy was, therefore, selected to represent the frequency characteristic of the vibration. The fundamental frequencies of three models and the corresponding pretension forces are listed in Table 4. The parameters of rigid body motion used in the case studies are shown in Table 5.

Table 4. Fundamental frequencies and pretension forces of different models.

Model	Frequencies/Hz	Pretension in x Direction/N	Pretension in y Direction/N
M1	0.50	0.147	0.25
M2	1.00	0.59	1
M3	2.00	3.1	3.7

Table 5. Parameters of rigid body motion.

Initial Rotational Velocity ω_0/(rad·s^{-1})	Deceleration Duration T/s		
$\pi/2$		1	
$\pi/5$	0.1	1	2
$\pi/100$		1	

Firstly, the dynamic responses of different models with the same rigid body motion are analyzed. The initial rotational velocity $\omega_0 = \pi/100$ (rad/s), the deceleration duration $T = 0.1$ s. The time histories of point A are shown in Figure 8 and the dynamic response frequencies and amplitudes are shown in Table 6. It can be observed that under the same rigid body motion, the dynamic response frequency of the membrane antenna is positively correlated with the fundamental frequency of the structure, while the maximum amplitude is negatively correlated with the fundamental frequency of the structure.

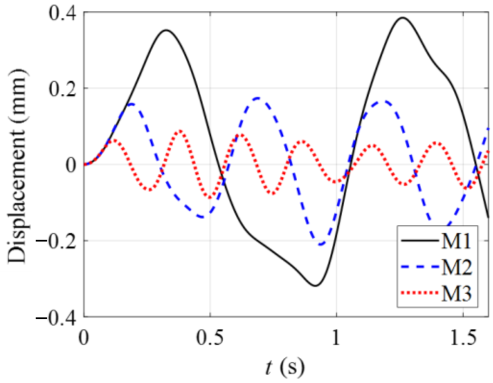

Figure 8. Time histories of point A of M1~M3, $\omega_0 = \pi/100$ (rad/s), $T = 0.1$.

Table 6. Dynamic responses of point A of M1~M3, $\omega_0 = \pi/100$ (rad/s), $T = 0.1$ s.

Model	Fundamental Frequency/Hz	Response Frequency/Hz	Amplitude/mm
M1	0.5003	0.9537	0.4441
M2	1.0005	2.0027	0.2101
M3	2.0000	3.9101	0.0871

Then, the dynamic responses of model M3 with the same initial rotational velocity ω_0 but different deceleration duration T are discussed. Assume that $\omega_0 = \pi/5$ (rad/s), $T = 0.1$ s, 1 s and 2 s, the time histories of point A are shown in Figure 9 and the dynamic response frequencies and amplitudes are shown in Table 7. One can find that with the increase of T, the response frequency and amplitude decrease, and the nonlinearity of the system becomes obvious. It also shows that the inertia force creates a new balanced position for nodes of the membrane antenna, instead of the plane before maneuvering. This is the reason why the displacement of A keeps positive before rigid motion stops.

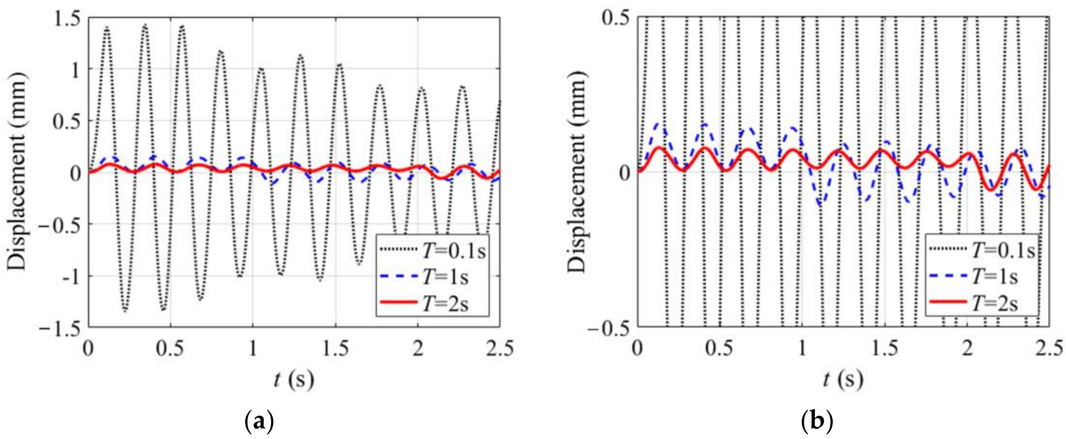

Figure 9. Time histories of point A of M3, $\omega_0 = \pi/5$ (rad/s). (**a**) The overall responses. (**b**) The details of the responses.

Table 7. Dynamic responses of point A of M3, $\omega_0 = \pi/5$ (rad/s).

Deceleration Duration T/s	Response Frequency/Hz	Amplitude/mm
0.1	4.1504	1.412
1	3.7231	0.1549
2	3.6621	0.0773

Next, the dynamic responses of model M1 with different initial rotational velocity ω_0 but the same deceleration duration T are discussed. Assume that $\omega_0 = \pi/2$ (rad/s), $\pi/5$ (rad/s) and $\pi/100$ (rad/s), the deceleration duration $T = 0.1$ s. The time histories of point A of the three cases are shown in Figure 9 and the dynamic response frequencies and amplitudes are shown in Table 8. It is obvious that the response frequency decreases with the decrease of initial rotational velocity ω_0. Additionally, the vibration amplitude evidently declines with the decrease of ω_0. From the discussion above we can draw the following conclusion: (1) the response frequency and vibration amplitude of the membrane antenna is strongly influenced by acceleration of the rigid body motion, i.e., for the same model, a larger acceleration will lead to a higher response frequency and a larger vibration amplitude; (2) the energy of vibration is dominated by the initial kinetic energy of the membrane antenna, i.e., for the same model, a larger initial rotational velocity will contribute to a larger vibration amplitude.

Table 8. Dynamic responses of point A of M1, $T = 0.1$ s.

Initial Rotational Velocity ω_0/(rad·s^{-1})	Response Frequency/Hz	Amplitude/mm
$\pi/2$	2.3842	6.3172
$\pi/5$	1.7166	3.9360
$\pi/100$	0.9537	0.4441

In Figure 10 and Table 8, the influence of initial velocity and deceleration duration have been discussed. We assume that the antenna rotates with the same initial velocity but different deceleration duration, or with different initial velocity but the same deceleration duration. However, there is another case that needs to be discussed, i.e., the antenna rotates with different initial velocity and different deceleration duration, but the same acceleration. Assume that the membrane antenna rotates in the following two cases: (1) $\omega_0 = \pi/5$ (rad/s), $T = 1$ s; (2) $\omega_0 = \pi/50$ (rad/s), $T = 0.1$ s. The time histories of point A are shown in Figure 11 and the dynamic response frequencies and amplitudes are shown in Table 9.

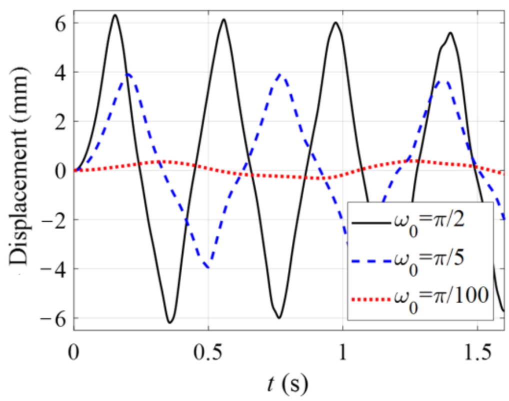

Figure 10. Time histories of point A of M1, $T = 0.1$ s.

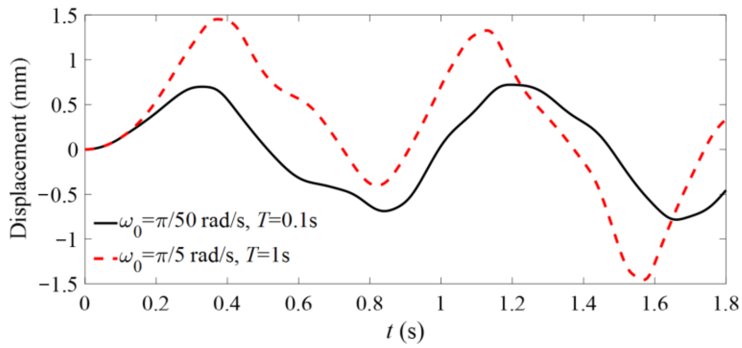

Figure 11. Time histories of point *A* of M1 with the same acceleration.

Table 9. Dynamic responses of point *A* of M1 with the same acceleration.

ω_0/(rad·s^{-1})	*T*/s	Response Frequency/Hz	Amplitude/mm
$\pi/5$	1	1.2398	1.4542
$\pi/50$	0.1	1.0490	0.7831

From Table 9, one can find that although the accelerations of the two cases are the same, the dynamic responses are still different. The amplitude and response frequency are larger when the initial rotational velocity is $\pi/5$ (rad·s^{-1}). Therefore, under the condition of the same acceleration, the initial velocity has more influence on the rigid–flexible coupling response than the deceleration duration.

It can be seen from the above case studies that the rigid body motion has a significant influence on the dynamic response characteristics of the space membrane antenna due to the rigid–flexible coupling effect, and the influence is related to the modal characteristics of the structure. For three models M1, M2 and M3, with different fundamental frequencies, the detailed influences of rigid motion on the dynamic response of the antenna are displayed in Figures 12 and 13.

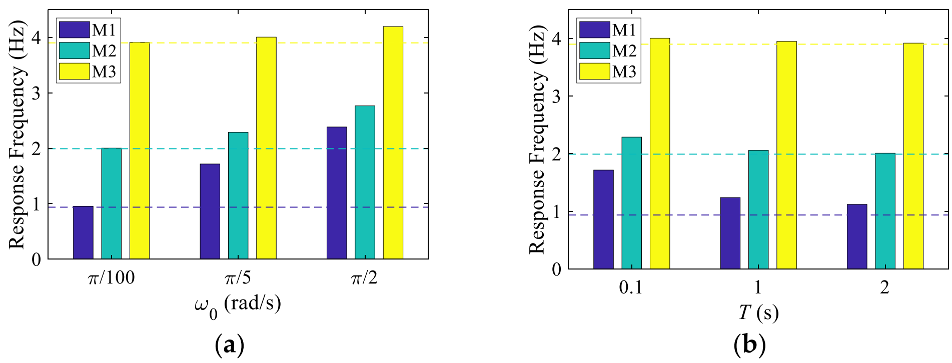

Figure 12. Relationship between response frequency and rigid body motion of different models. (**a**) T = 0.1 s with different ω_0 (**b**) $\omega_0 = \pi/5$ (rad/s) with different *T*.

The blue, green, and yellow dotted lines in Figure 12 denote the natural frequencies of the dominant mode (fourth-order mode) of models M1, M2 and M3, which are 0.94 Hz, 1.99 Hz and 3.90 Hz, respectively. It can be found that the response frequency increases with the increase of the fundamental frequency of the model. At the same time, the rigid–flexible coupling response frequency of the structure climbs with the increase of the rigid body motion acceleration. When the acceleration approaches zero, the influence of the rigid–flexible coupling effect decreases significantly, and the structural response frequency approaches the natural frequency of the dominant mode. From Figure 13, one can find that the vibration amplitude of the structure decreases with the increase of fundamental frequency and deceleration duration, and increases with the increasing of initial velocity.

Comparatively speaking, the initial kinetic energy of the structure dominantly determines the maximum vibration amplitude that could be achieved. In addition, by comparing the three models, the response frequency of M1 is significantly affected by the initial velocity and deceleration duration, while the influence on M3 is relatively weak. This means that under the same rigid body motion condition, the rigid–flexible coupling effect will have a stronger influence on the structure with lower fundamental frequency.

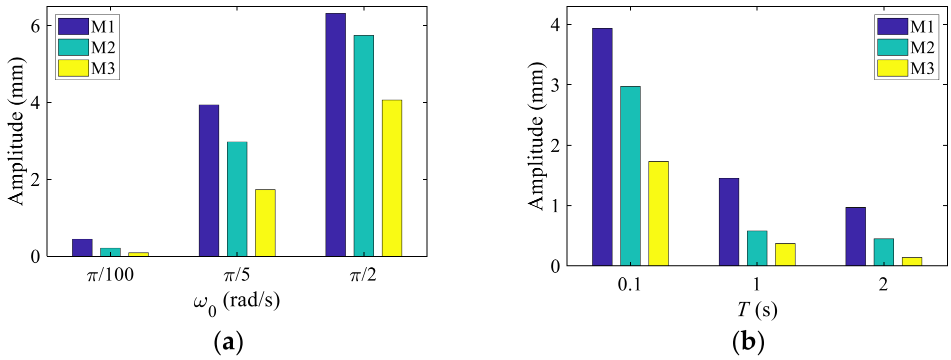

Figure 13. Relationship between vibration amplitude and rigid body motion of different models. (**a**) T = 0.1 s with different ω_0 (**b**) $\omega_0 = \pi/5$ (rad/s) with different T.

5. Conclusions

In this study, a rigid–flexible coupling nonlinear dynamic finite element model of a maneuvering space pretensioned membrane antenna is established. Based on the numerical simulation results, the influence of rigid body motion and structural dynamic characteristics on the dynamic response of membrane antenna is investigated. Conclusions are as follows.

(1) The acceleration of rigid body motion provides new stiffness and damping component to membrane structures, which is called dynamic impedance. It can be learnt from the model derivation, that rigid–flexible coupling effect is proportional to acceleration and square of velocity of rigid motion. Overall, the frequency increment relative to the response modal frequency will increase and the vibration amplitude will decrease as the initial rotational velocity and acceleration grow.

(2) The frequency increment and the vibration amplitude are under a combined impact caused by linear and nonlinear stiffness of the structure as well as rigid–flexible coupling effect. For a membrane antenna with a fundamental frequency of 0.5 Hz, when its rotational velocity is magnified 10 times, the frequency increment and amplitude are about 2.7 times and 1.86 times larger than before, respectively; and when its acceleration is increased 10 times, the frequency increment and amplitude are around 2.57 times and 2.7 times smaller than before, respectively.

(3) The rigid–flexible coupling effect can be more notable for the membrane structure with a smaller fundamental frequency. When the fundamental frequency is halved, the response frequency increment induced by rigid–flexible coupling effect will be doubled, while the amplitude will decrease whose reduction proportion is positively correlated with the acceleration.

Author Contributions: Conceptualization, Y.L.; formal analysis, Q.S.; investigation, G.F.; methodology, Q.S.; project administration, L.L.; supervision, H.Y.; writing—original draft, Y.L. and Q.S.; writing—review and editing, Y.L. All authors have read and agreed to the published version of the manuscript.

Funding: This research was funded by the National Natural Science Foundation of China (No. 52005125), the Young Elite Scientists Sponsorship Program by CAST (YESS20210134), the Fundamental Research Funds for the Central Universities, China (No. FRFCU5710050921) and Open Project of Space Structure and Mechanism Technology Laboratory of China Aerospace Science and Technology Group Co., Ltd.

Conflicts of Interest: The authors declare no conflict of interest.

References

1. Zheng, Z.L.; Liu, C.J.; He, X.T.; Chen, S.L. Free Vibration Analysis of Rectangular Orthotropic Membranes in Large Deflection. *Math. Probl. Eng.* **2009**, *2009*, 634362. [CrossRef]
2. Zheng, Z.L.; Liu, C.Y.; Li, D.; Zhang, T. Dynamic response of orthotropic membrane structure under impact load based on multiple scale perturbation method. *Lat. Am. J. Solids Struct.* **2017**, *14*, 1490–1505. [CrossRef]
3. Zheng, Z.L.; Song, W.J.; Liu, C.J.; He, X.T.; Sun, J.Y.; Xu, Y.P. Study on dynamic response of rectangular orthotropic membranes under impact loading. *J. Adhes. Sci. Technol.* **2012**, *26*, 1467–1479. [CrossRef]
4. Liu, C.J.; Zheng, Z.L.; Yang, X.Y.; Zhao, H. Nonlinear damped vibration of pre-stressed orthotropic membrane structure under impact loading. *Int. J. Struct. Stab. Dyn.* **2014**, *14*, 1350055. [CrossRef]
5. Liu, C.J.; Zheng, Z.L.; Yang, X.Y.; Guo, J.J. Geometric Nonlinear Vibration Analysis for Pretensioned Rectangular Orthotropic Membrane. *Int. Appl. Mech.* **2018**, *54*, 104–119. [CrossRef]
6. Sunny, M.; Kapania, R.; Sultan, C. Solution of the Nonlinear Transverse Vibration Problem of a Prestressed Membrane Using the Adomian Decomposition Method. In Proceedings of the 52nd AIAA/ASME/ASCE/AHS/ASC Structures, Structural Dynamics and Materials Conference, Denver, Colorado, 4–7 April 2011; American Institute of Aeronautics and Astronautics: Reston, VA, USA, 2011; pp. 1–17.
7. Fang, H.; Yang, B.; Ding, H.; Hah, J.; Quijano, U.; Huang, J. Dynamic analysis of large in-space deployable membrane antennas. In Proceedings of the 13th International Congress on Sound and Vibration, Vienna, Austria, 2 July 2006; Volume 6, pp. 5133–5140.
8. Liu, X.; Cai, G.P.; Peng, F.J.; Zhang, H.; Lv, L.L. Nonlinear vibration analysis of a membrane based on large deflection theory. *JVC/J. Vib. Control* **2018**, *24*, 2418–2429. [CrossRef]
9. Liu, X.; Cai, G.; Peng, F.; Zhang, H. Active control of large-amplitude vibration of a membrane structure. *Nonlinear Dyn.* **2018**, *93*, 629–642. [CrossRef]
10. Liu, X.; Cai, G.; Peng, F.; Zhang, H. Nonlinear vibration control of a membrane antenna structure. *Proc. Inst. Mech. Eng. Part G J. Aerosp. Eng.* **2019**, *233*, 3273–3285. [CrossRef]
11. Zhang, J.; Rui, X.; Li, B.; Chen, G. Study on the Stress-Stiffening Effect and Modal Synthesis Methods for the Dynamics of a Spatial Curved Beam. *J. Appl. Mech. Trans. ASME* **2016**, *83*, 081004. [CrossRef]
12. Deng, F.; He, X.; Li, L.; Zhang, J. Dynamics modeling for a rigid-flexible coupling system with nonlinear deformation field. *Multibody Syst. Dyn.* **2007**, *18*, 559–578. [CrossRef]
13. Yoo, H.H.; Chung, J. Dynamics of rectangular plates undergoing prescribed overall motion. *J. Sound Vib.* **2001**, *239*, 123–137. [CrossRef]
14. Fan, J.; Zhang, D.; Shen, H. Discretization Methods of a Rotating Flexible Rectangular Thin Plate. *J. Shanghai Jiaotong Univ.* **2020**, *25*, 118–126. [CrossRef]
15. Yuan, Q.; Liu, Y.; Qi, N. Active vibration suppression for maneuvering spacecraft with high flexible appendages. *Acta Astronaut.* **2017**, *139*, 512–520. [CrossRef]
16. Liu, L.; Cao, D.; Wei, J.; Tan, X.; Yu, T. Rigid-Flexible Coupling Dynamic Modeling and Vibration Control for a Three-Axis Stabilized Spacecraft. *J. Vib. Acoust.* **2017**, *139*, 041006. [CrossRef]
17. Li, Q.; Ma, X.; Wang, T. Reduced Model for Flexible Solar Sail Dynamics. *J. Spacecr. Rockets* **2011**, *48*, 446–453. [CrossRef]
18. Zhang, J.; Wang, T. Coupled attitude-orbit control of flexible solar sail for displaced solar orbit. *J. Spacecr. Rockets* **2013**, *50*, 675–685. [CrossRef]
19. Liu, J.; Cui, N. Rigid–flexible coupled dynamics analysis for solar sails. *Proc. Inst. Mech. Eng. Part G J. Aerosp. Eng.* **2019**, *233*, 324–340. [CrossRef]
20. Song, M.; Renson, L.; Noël, J.P.; Moaveni, B.; Kerschen, G. Bayesian model updating of nonlinear systems using nonlinear normal modes. *Struct. Control Health* **2018**, *25*, e2258. [CrossRef]
21. Trujillo-Franco, L.G.; Silva-Navarro, G.; Beltran-Carbajal, F. Algebraic Parameter Identification of Nonlinear Vibrating Systems and Non Linearity Quantification Using the Hilbert Transformation. *Math Probl. Eng.* **2021**, *2021*, 5595453. [CrossRef]
22. Habib, G.; Cirillo, G.I.; Kerschen, G. Isolated resonances and nonlinear damping. *Nonlinear Dyn.* **2018**, *93*, 979–994. [CrossRef]
23. Li, Y.L.; Lu, M.Y.; Tan, H.F.; Tan, Y.Q. A study on wrinkling characteristics and dynamic mechanical behavior of membrane. *Acta Mech. Sin. Xuebao* **2012**, *28*, 201–210. [CrossRef]
24. Shi, H.; Wang, C.; Liu, L.; Gao, Z.; Xie, Y. An active control strategy to suppress nonlinear vibrations of large space membranes. *Acta Astronaut.* **2019**, *155*, 80–89. [CrossRef]
25. Kane, T.R.; Ryan, R.R.; Banerjee, A.K. Dynamics of a cantilever beam attached to a moving base. *J. Guid. Control. Dyn.* **1987**, *10*, 139–151. [CrossRef]
26. Rizzi, S.A.; Przekop, A. System identification-guided basis selection for reduced-order nonlinear response analysis. *J. Sound Vib.* **2008**, *315*, 467–485. [CrossRef]
27. Allemang, R.J.; Brown, D.L. A Correlation Coefficient for Modal Vector Analysis. *Proc. Int. Conf.* **1982**, 110–116. [CrossRef]